Available online at www.sciencedirect.com
ScienceDirect
Trans. Nonferrous Met. Soc. China 34(2024) 3486−3503
Transactions of Nonferrous Metals Society of China
www.tnmsc.cn

Improvement of microstructure and mechanical properties of Al−Cu−Li−Mg−Zn alloys through water-cooling centrifugal casting technique

Qing-bo YANG[1,2,3], Wen-jing SHI[1], Wen LIU[2], Miao WANG[2], Wen-bo WANG[2], Li-na JIA[1,2], Hu ZHANG[1,2]

1. School of Materials Science and Engineering, Beihang University, Beijing 100191, China;
2. Research Center for Lightweight Materials, Ningbo Institute of Technology, Beihang University, Ningbo 315100, China;
3. Suzhou Laboratory, Suzhou 215123, China

Received 10 June 2023; accepted 28 February 2024

Abstract: The microstructure and mechanical properties of as-cast Al−Cu−Li−Mg−Zn alloys fabricated by conventional gravity casting and centrifugal casting techniques combined with rapid solidification were investigated. Experimental results demonstrated that compared with the gravity casting technique, the water-cooling centrifugal casting technique significantly reduces porosity, refines α(Al) grains and secondary phases, modifies the morphology of secondary phases, and mitigates both macro- and micro-segregation. These improvements arise from the synergistic effects of the vigorous backflow, centrifugal field, vibration and rapid solidification. Porosity and coarse plate-like $Al_{13}Fe_4$/Al_7Cu_2Fe phase result in the fracture before the gravity-cast alloy reaches the yield point. The centrifugal-cast alloy, however, exhibits an ultra-high yield strength of 292.0 MPa and a moderate elongation of 6.1%. This high yield strength is attributed to solid solution strengthening (SSS) of 225.3 MPa, and grain boundary strengthening (GBS) of 35.7 MPa. Li contributes the most to SSS with a scaling factor of 7.9 MPa·wt.%$^{-1}$. The elongation of the centrifugal-cast alloy can be effectively enhanced by reducing the porosity and segregation behavior, refining the microstructure and changing the morphology of secondary phases.

Key words: Al−Cu−Li−Mg−Zn alloy; water-cooling centrifugal casting; microstructure; mechanical properties; segregation behavior

1 Introduction

The pursuit of advanced lightweight materials with exceptional mechanical properties is of paramount importance in a wide range of industries, particularly in aerospace, aviation, and defense. Among these materials, the third-generation Al−Li alloys, exemplified by the Al−Cu−Li−Mg−Ag alloy, have gained attention owing to their excellent combination of low density, high specific strength and stiffness, fracture toughness, corrosion resistance and weldability [1−3]. Recently, a strategic focus has been directed towards substituting Ag with Zn, resulting in the development of the Al−Cu−Li−Mg−Zn alloy. This alloy not only achieves cost reduction due to the lower cost of Zn compared to Ag but also demonstrates exceptional mechanical properties [4]. In the T8 temper condition, the Al−Cu−Li−Mg−Zn alloy exhibits remarkable mechanical properties such as an ultimate tensile strength (UTS) of 753 MPa, a yield strength (YS) of

Corresponding author: Li-na JIA, E-mail: jialina@buaa.edu.cn;
Hu ZHANG, E-mail: zhanghu@buaa.edu.cn
DOI: 10.1016/S1003-6326(24)66621-5

731 MPa and an elongation (EL) of 5.5% [4].

In the fabrication of this ultra-high strength Al−Cu−Li−Mg−Zn alloy, casting techniques play a critical role, setting the stage for the subsequent heat treatments and deformation processes. These casting techniques not only efficiently produce components with complex shapes but also mitigate the anisotropy of mechanical properties. However, traditional casting methods often yield microstructures characterized by coarse grains (a grain size ranging from dozens to thousands of microns), severe segregation, undesirable secondary phases and porosity defects [5]. These microstructural imperfections persist by subsequent processing steps, leading to a substantial deterioration in the mechanical properties of the Al−Li alloy. Consequently, achieving fine and homogenous microstructures is essential, especially to meet the demands for lightweight and robust components.

Efforts to improve the microstructure and mechanical properties of as-cast alloys have centered on rapid solidification technique and external forces during solidification [6,7]. Due to their high nucleation rates, the rapid solidification technique offers a pathway to refine grains. This is exemplified in the case of aluminum alloys such as AA2195, wherein the application of rapid solidification processing results in the formation of fine and homogeneous microstructures, subsequently contributing to outstanding mechanical properties [8]. In addition to the rapid solidification technique, external physical fields including mechanical stirring, supersonic vibration, magnetic field and centrifugal force have yielded promising outcomes in grain refinement during solidification [6,9,10]. Ultrasonic treatment significantly reduces the grain size, homogeneously disperses secondary phases and enhances strength and elongation (EL) in the Al−5Cu−0.6Li−0.5Mn−0.3Mg−0.15Ti alloy [9]. The application of static magnetic, pulse electric, and electromagnetic oscillation fields has proven to be effective in reducing dendrites, mitigating central segregation, and minimizing eutectic phase count. This comprehensive optimization in microstructure results in a noteworthy enhancement of the alloy's overall mechanical properties [6]. TIAN et al [10] employed centrifugal casting technology followed by subsequent hot-deformation and artificial aging processes to achieve a high-strength, low-anisotropy Al−Li plate with fine α(Al) grains and secondary phases. Among various external forces, the centrifugal casting technique emerges as a particularly intriguing approach. This method utilizes centrifugal force to exert pressure, facilitating the injection of molten metal into a swiftly rotating mold. The resulting centrifugal casting manifests a refined microstructure, superior density, excellent surface finish, and elevated mechanical properties. The exploration of these external forces has demonstrated promising outcomes, signifying their potential in tailoring the microstructure of Al alloys.

The combination of rapid solidification and centrifugal casting methods constitutes a multifaceted approach in the quest to optimize the microstructure and mechanical properties of as-cast Al alloys. However, there remains a notable scarcity of systematic investigations into the microstructure and mechanical properties of the as-cast Al−Cu−Li− Mg−Zn alloy manufactured through the centrifugal casting technique combined with the rapid solidification.

In light of these considerations, in this study, the fabrication of the as-cast Al−Cu−Li−Mg−Zn alloy through the innovative combination of rapid solidification and centrifugal casting technique was investigated. The objective was to attain a fine and homogenous microstructure with minimal compositional segregation, leading to exceptionally high mechanical properties. Additionally, the differences in the microstructure and mechanical properties of the Al−Cu−Li−Mg−Zn alloy produced by both gravity casting and water-cooled centrifugal casting techniques were compared.

2 Experimental

2.1 Casting process

The centrifugal casting setup is schematically depicted in Fig. 1(a). The apparatus includes an infrared thermometer, a water-cooled copper mold, a graphite crucible, an induction heater, a rotation axis, a casting chamber and a balance. The interconnected graphite crucible and copper mold experience high-speed rotation facilitated by the revolving axis.

The initial ingot, composed of Al−4Cu−3Li−0.7Mg−1Zn (wt.%), was subjected to heating and melting in a graphite crucible using the induction

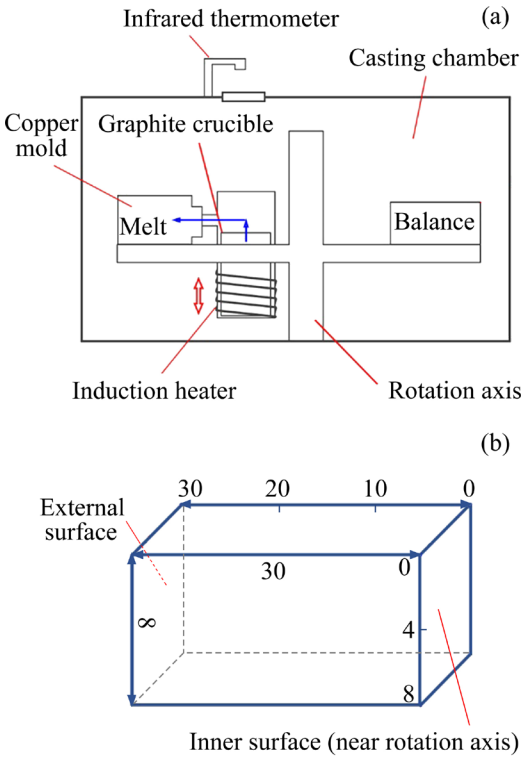

Fig. 1 Schematic illustration of centrifugal casting machine (a) and cast billet (b) (Unit: mm)

heater. The molten metal was held at a temperature of 750 °C for approximately 5 min. Subsequently, the molten metal was poured into the copper mold by centrifugal force and finally solidified. The molten metal was directed towards the central section of the copper mold, as indicated by blue arrows in Fig. 1(a). The whole experimental process was kept in an environment of inert argon gas to protect the molten metal. The casting parameters were as follows: a casting temperature of 730 °C, a rotation speed of 700 r/min, and a water flow rate of approximately 18 L/min. An infrared thermometer was positioned on top of the casting chamber to measure the melt temperature. In gravity casting, an identical remelting process was employed as in centrifugal casting; however, the molten metal was manually poured into the copper mold. The gravity-cast and centrifugal-cast alloys have dimensions of approximately 30 mm in length, 20 mm in width and 8 mm in height.

The alloy compositions of the initial ingot, gravity-cast and centrifugal-cast Al−Cu−Li−Mg−Zn alloys were measured by an inductively coupled plasma emission spectrometer (ICP-OES) and are listed in Table 1.

Table 1 Chemical compositions of Al−Cu−Li−Mg−Zn alloy

Specimen	Content/wt.%						
	Cu	Li	Mg	Zn	Fe	Zr	Al
Initial ingot	4.40	3.00	0.70	1.10	0.14	0.1	Bal.
Gravity casting	4.10	2.91	0.60	1.08	0.12	0.08	Bal.
Centrifugal casting	4.09	2.89	0.61	1.05	0.14	0.07	Bal.

2.2 Characterization methods

The microstructures of gravity-cast and centrifugal-cast alloys were investigated employing various techniques including optical metallography (OM), electron probe microanalysis (EPMA), scanning electron microscopy (SEM), X-ray diffraction (XRD) and transmission electron microscopy (TEM). Macro-segregation tests were conducted on the cast billet in both horizontal (0, 10, 20 and 30 mm from the inner to outer surface) and vertical (0, 4 and 8 mm from the top to bottom) directions. The terms “4 mm-inner” and “4 mm-outer” specifically referred to the inner and outer of the 4 mm position, as shown in Fig. 1(b), respectively. SEM and OM micrographs were analyzed using ImageJ software to determine the volume fraction, size of secondary phases and grains, and porosity area fraction. Secondary phases were identified using XRD with a D/Max2500pc X-ray diffractometer equipped with a Cu K_α radiation source, operating at a scanning rate of 2 (°)/min. Further characterization of secondary phases was employed using a JEM−2100 TEM equipped with selected area electron diffraction (SAED). TEM specimens were pre-thinned using conventional mechanical grinding and polishing to get 3 mm-diameter disks. The disks were then twin-jet polished using a solution of 30 vol.% nitric acid and 70 vol.% methanol at a temperature between −25 and −34 °C. Tensile tests were performed at room temperature using a universal electronic tensile testing machine with a constant strain rate of 1.0×10^{-3} s^{-1}. Three parallel tests were performed to verify the reproducibility of the results.

3 Results

3.1 Microstructure

Metallographic analysis results of the different sections of Al−Cu−Li−Mg−Zn alloys produced by

both gravity and centrifugal casting techniques are presented in Fig. 2. The gravity-cast alloy shows an inhomogeneous solidification microstructure with large equiaxed α(Al) grains enveloped by semi-continuous eutectic phases, which is the typical dendrite growth mode (pink arrows in Figs. 2(a−d)). Although microstructural features are similar at the 4 mm-inner and 4 mm-outer positions (Figs. 2(b, d)), a progressive increase in the number of coarse dendritic structures is observed with decreasing height (Figs. 2(a−c)). However, the centrifugal-cast alloy at different positions consists of a relatively homogeneous solidification microstructure with small equiaxed α(Al) grains and continuous eutectic phases in the intercellular/dendritic regions (Figs. 2(e−h)). Additionally, fine dendritic structures are present, with a slight increase in their quantity from the 4 mm-inner to 4 mm-outer regions (Figs. 2(f, h)).

The typical size distributions based on at least 1000 grains in various sample locations are analyzed by ImageJ software, as shown in the histograms of Fig. 3. The gravity casting shows a wide grain size distribution with 87% of investigated

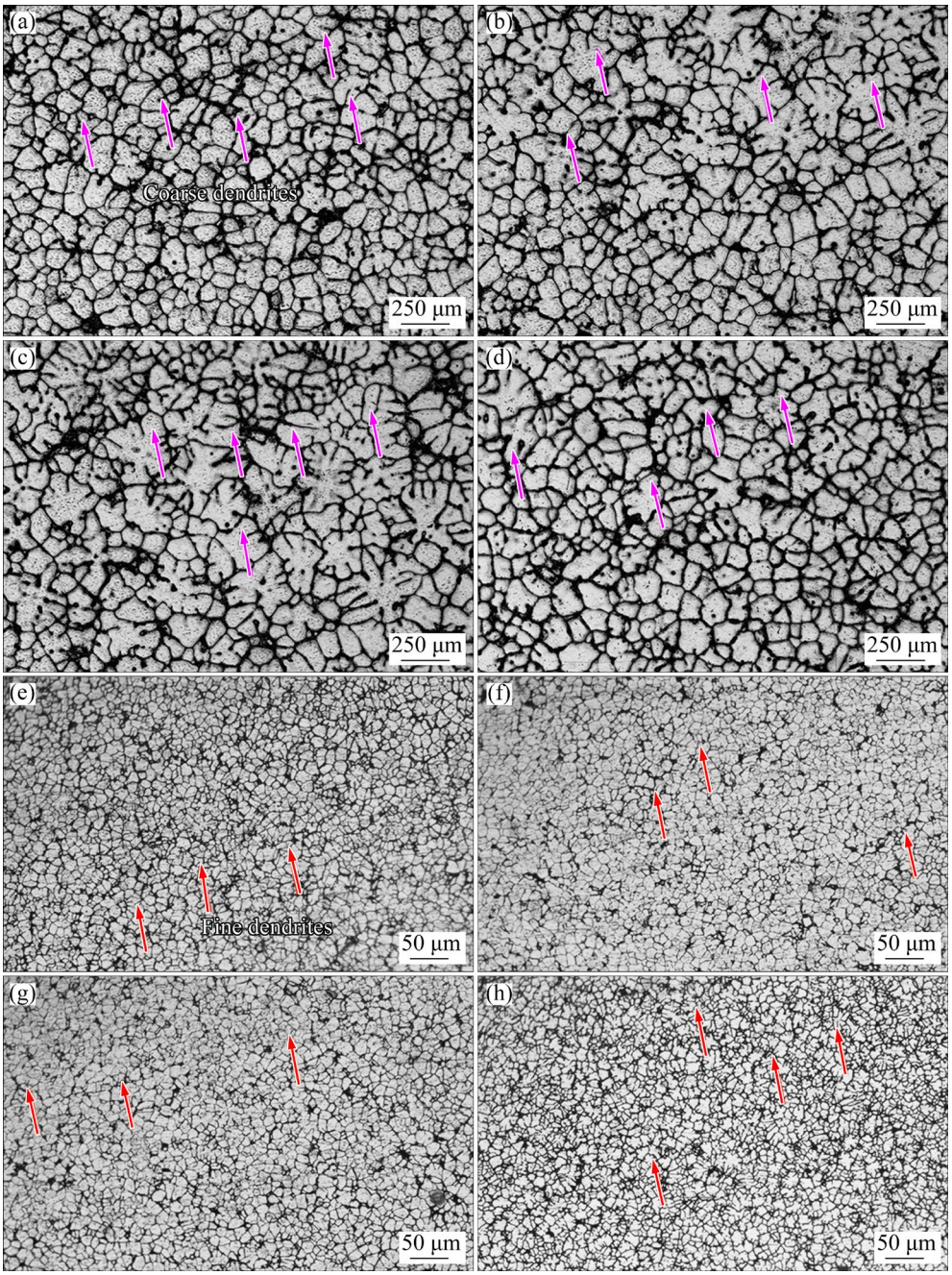

Fig. 2 OM images of gravity (a−d) and centrifugal (e−h) castings at different positions: (a, e) 0 mm; (b, f) 4 mm-inner; (c, g) 8 mm; (d, h) 4 mm-outer

grains ranging from 52.2 to 209.4 μm. The centrifugal-cast alloy, however, exhibits a relatively narrow grain size distribution with 86% of analyzed grains in the range of 4.0−13.4 μm. The average grain size is 131.6 μm for the gravity casting and 9.7 μm for the centrifugal casting.

3.2 Segregation behavior

3.2.1 Macro-segregation

The solidification process in both gravity-cast and centrifugal-cast alloys inevitably leads to macro-segregation of alloying elements, impacting both microstructural uniformity and mechanical properties. Figure 4 depicts the mass fractions of Cu, Mg, Zn and Fe elements at different positions in both gravity and centrifugal castings. The mass fractions of the same element at different locations generally exhibit similar trends, demonstrating the precision and repeatability of the experimental data. Owing to differences in density, Cu, Zn and Fe elements in gravity casting exhibit a predominant concentration towards the bottom, while the Mg element segregates towards the top. This indicates significant gravity-induced segregation along the vertical direction (Figs. 4(a−d)). Moreover, Cu, Mg, Zn and Fe elements of the gravity casting exhibit a modest horizontal segregation characteristic.

In contrast, the mass fractions of Cu, Mg, Zn, and Fe elements in the centrifugal casting along the vertical direction (Figs. 4(e−h)) reveal minimal concentration disparities, which indicates minor gravitational segregation. The profiles of Cu, Zn and Fe elements all display modest upward tendencies, whereas those of Mg exhibit a slight downward trend along the horizontal direction. The degree of macro-segregation of Cu, Mg, Zn and Fe elements along the centrifugal force direction is less conspicuous compared with the horizontal segregation observed in the gravity-cast alloy. However, a slight range of variation persists spanning from 0.1 wt.% to 0.2 wt.%, which indicates a modest degree of macro-segregation along the centrifugal force direction. Additionally, the centrifugal-cast alloy shows minor fluctuations across diverse positions, which illustrates the homogeneous distribution of Cu, Mg, Zn and Fe elements. In contrast, pronounced fluctuations of the gravity-cast alloy at various positions signify the non-uniform distribution of these elements.

3.2.2 Micro-segregation

The concentration slope ratio (CSR) is regarded as a crucial indicator for evaluating the extent of micro-segregation of solute elements. Points P_1, P_2 and P_3 are distributed along a straight line within the gravity-cast alloy as shown in Fig. 5(a), which is used to calculate CSR using the relationship provided below [6]:

$$\mathrm{CSR}=k_1/k_2=\frac{c_1-c_2}{l_2-l_1}\Big/\frac{c_2-c_3}{l_3-l_2}=\frac{c_1-c_2}{c_2-c_3}\cdot\frac{l_3-l_2}{l_2-l_1} \quad (1)$$

where k_1 and k_2 are the concentration gradients of solute elements between Points P_1 and P_2, and Points P_2 and P_3, respectively; c_1, c_2 and c_3 are the solute concentrations at P_1, P_2 and P_3 points, respectively; l_1, l_2 and l_3 represent the distance from the eutectics to Points P_1, P_2 and P_3, respectively.

When CSR is greater than 1, the degree of micro-segregation of solute elements increases with the increase of CSR. The CSR of Cu, Mg, Zn and Fe elements at various positions of gravity and centrifugal castings is shown as histograms in Figs. 5(b) and (c) respectively. In gravity casting,

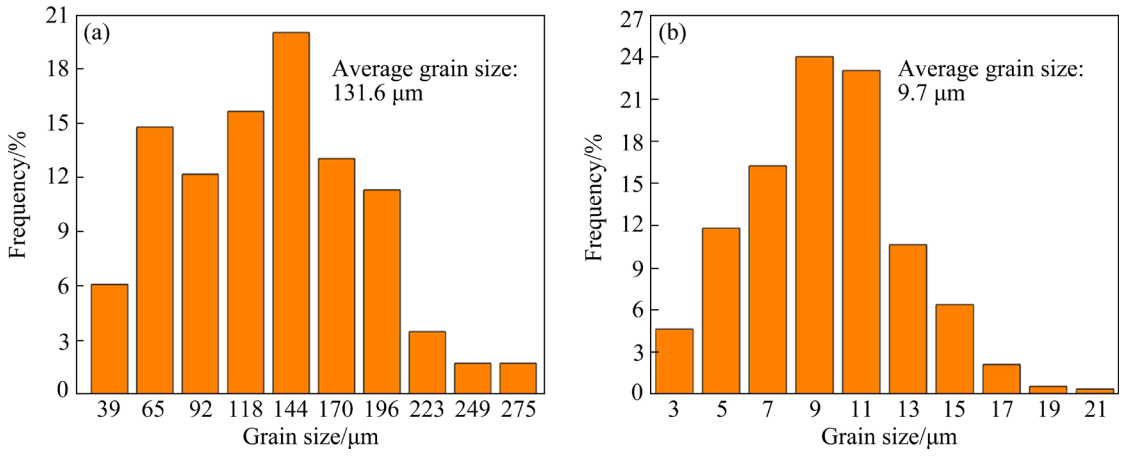

Fig. 3 Average grain size and size distribution of gravity-cast (a) and centrifugal-cast (b) alloys

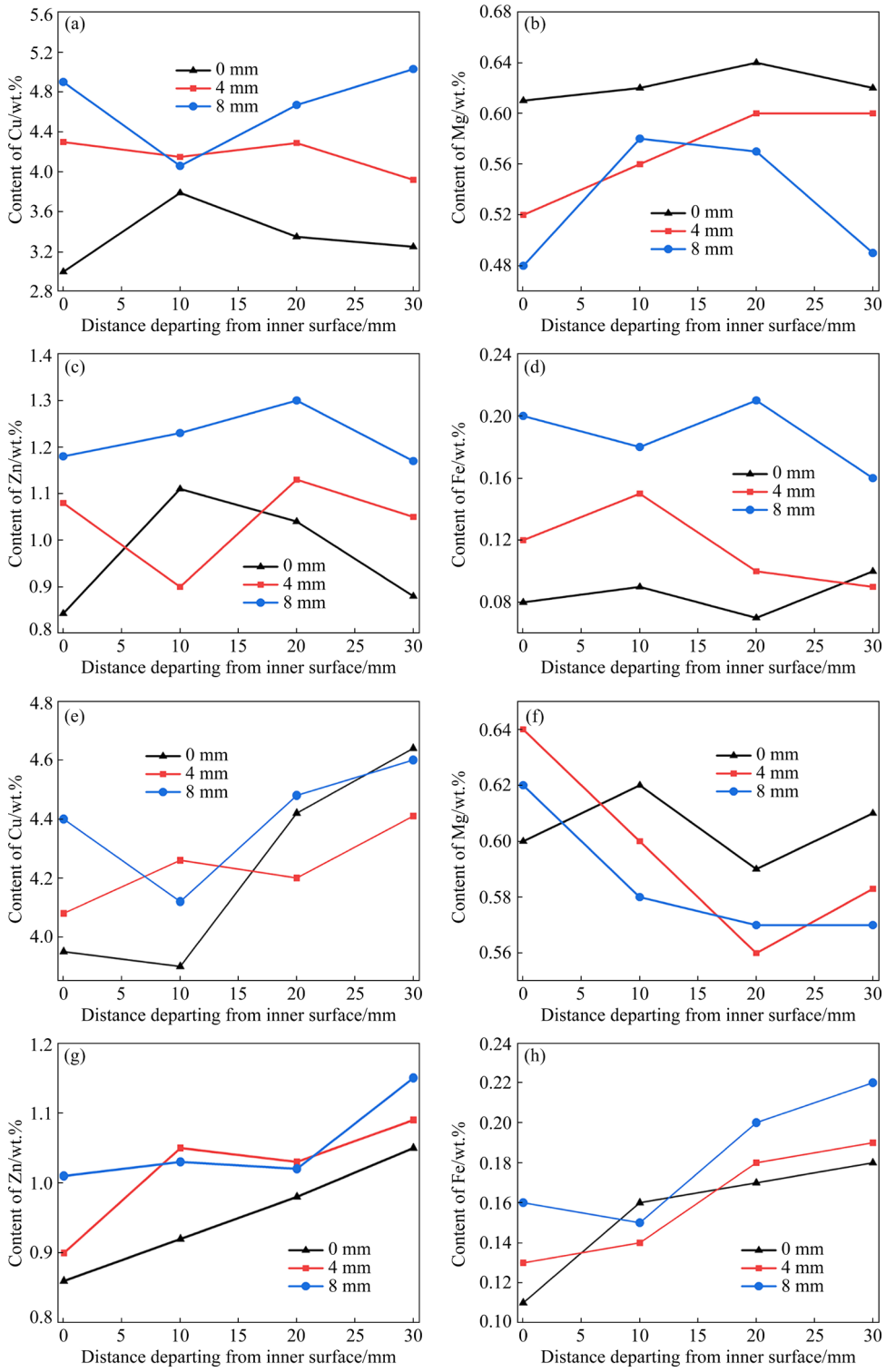

Fig. 4 Mass fractions of Cu, Mg, Zn, and Fe elements on different sections of gravity-cast (a−d) and centrifugal-cast (e−h) alloys

the CSR of Cu, Mg, Zn and Fe elements increases as the height decreases, while that at different positions in centrifugal casting remains relatively consistent. The average CSR of Cu, Mg, Zn and Fe elements in the gravity casting is 3.68, 3.58, 2.72 and 2.52, respectively, while that in the centrifugal casting is 2.10, 1.88, 1.92 and 1.89, respectively. Notably, the average CSR for Cu, Mg, Zn and Fe elements in centrifugal casting is consistently lower when compared to the analogous value calculated

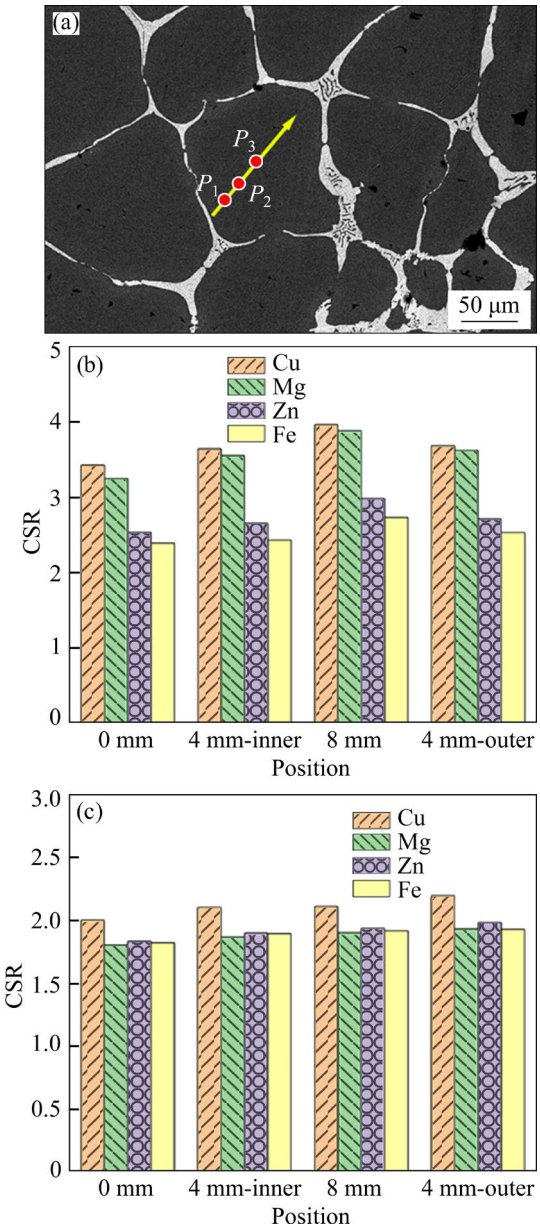

Fig. 5 Sequence of Positions P_1, P_2, and P_3 in straight line to calculate CSR (a) and values of CSR of gravity-cast (b) and centrifugal-cast (c) alloys

for gravity casting. Moreover, the average CSR of Cu, Mg and Zn elements in the centrifugal casting is also lower than that in the Al−Cu−Li−Mg−Zn alloy applied electromagnetic oscillation field during twin-roll casting (3.16, 2.64 and 1.93) [6]. High CSR indicates severe micro-segregation of solute elements during solidification. Therefore, compared to gravity casting and electromagnetic oscillation technologies, centrifugal casting technology can effectively mitigate the micro-segregation of Cu, Mg, Zn, and Fe elements, resulting in a homogenous distribution of these elements.

3.3 Characteristics of secondary phases

3.3.1 XRD patterns

The XRD analysis was conducted on both gravity-cast and centrifugal-cast alloys to verify the phase compositions, as shown in Fig. 6. The primary phases of all the gravity-cast alloys include α(Al), T_2(Al_6CuLi_3) and θ(Al_2Cu) phases, in conjunction with impurity phases ($Al_{13}Fe_4$ and Al_7Cu_2Fe) commonly associated with the presence of Fe elements. However, in all samples of the centrifugal-cast alloy, only α(Al), Al_6CuLi_3, Al_2Cu, and $Al_{13}Fe_4$ phases are present, with the notable absence of the Al_7Cu_2Fe phase. It is noteworthy that no characteristic diffraction peaks of Zn-bearing intermetallic phases such as η($MgZn_2$) and T(AlZnMgCu) phases in 7xxx series Al−Zn alloys [11] can be identified in both gravity-cast and centrifugal-cast alloys. This absence is attributed to the lower Zn content within the Al−Cu−Li−Mg−Zn alloy in contrast to the 7xxx series Al−Zn alloys.

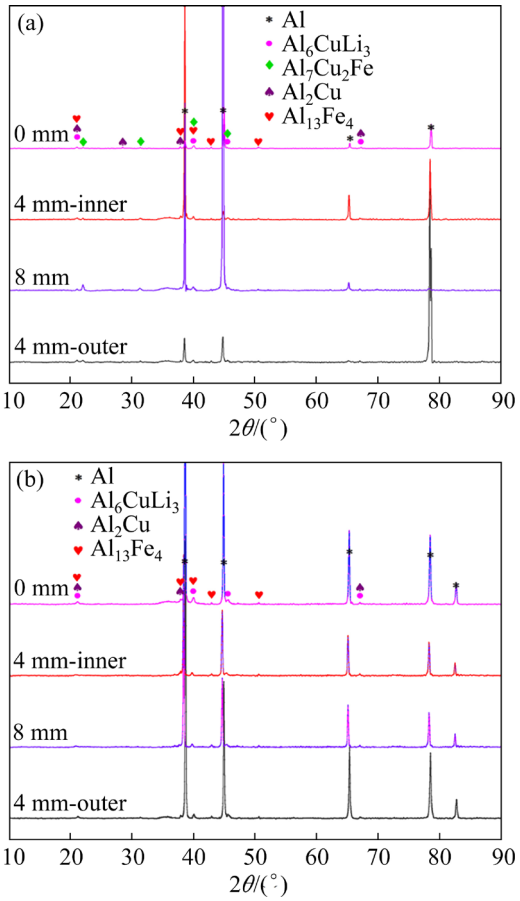

Fig. 6 XRD patterns of gravity (a) and centrifugal (b) castings

3.3.2 SEM and TEM images

The SEM micrographs of secondary phases on different sections of gravity-cast and centrifugal-cast alloys are shown in Figs. 7 and 8, respectively. The corresponding chemical compositions of secondary phases acquired through EDS or EPMA point analyses are listed in Table 2. In the gravity-cast alloy (Fig. 7), four distinct secondary phases are observed within the intercellular/dendritic regions. These phases are the α(Al)+Al_6CuLi_3 eutectic phase (Point G_1), Al_2Cu phase (Point G_2), $Al_{13}Fe_4$ phase (Point G_3) and Al_7Cu_2Fe phase (Point G_4). Interestingly, the Fe-containing intermetallic compounds exhibit a unique core−shell configuration (Fig. 7), with the $Al_{13}Fe_4$ phase forming the core encased by the Al_7Cu_2Fe phase shell. This core−shell structure results from an incomplete peritectic reaction involving the $Al_{13}Fe_4$ and liquid phases in the Al−Cu−Fe−Mg−Si alloy [12]. Additionally, a needle-shaped phase is also observed within the grain interior. Apart from secondary phases, the gravity-cast alloy displays a notable presence of small pores, contributing to a porosity area fraction of 0.29%. The centrifugal-cast alloy exclusively consists of the α(Al)+Al_6CuLi_3 eutectic phase (Point C_1), Al_2Cu phase (Point C_2) and $Al_{13}Fe_4$ phase (Point C_3), as demonstrated in Fig. 8. Notably, Al_7Cu_2Fe and needle-shaped phases are absent, with only a negligible number of small pores. The overall area fraction of porosity in the centrifugal-cast alloy amounts to 0.021%, significantly lower than that observed in the gravity-cast alloy. Moreover, it is extremely intriguing to notice that the $Al_{13}Fe_4$ phase grows individually in the centrifugal-cast alloy, which is significantly different from the core-shell structure in the gravity-cast alloy.

The quantitative information, such as the diameter/thickness of secondary phases in both gravity-cast and centrifugal-cast alloys, is listed in Table 3. In the gravity-cast alloy, the average diameter/thickness of the eutectic α(Al)+Al_6CuLi_3, Al_2Cu and $Al_{13}Fe_4$/Al_7Cu_2Fe phases is 4.38, 2.77 and 2.28 μm, respectively. However, in the centrifugal-cast alloy, the average diameter/thickness of these phases is markedly reduced, measuring 0.68, 0.41, and 0.28 μm, respectively. Compared with the gravity-cast alloy, the intermetallic compounds in the centrifugal-cast alloy are significantly refined and homogeneously distributed, as illustrated in Figs. 7 and 8, and Table 3. Moreover, irregular Al_2Cu (61.80%) and huge platelet-like $Al_{13}Fe_4$/Al_7Cu_2Fe (56.80%) phases prevail in the gravity casting, whereas spherical Al_2Cu (88.10%) and $Al_{13}Fe_4$ (98.10%) phases are predominant in the centrifugal casting (Table 4). This refinement, spheroidized morphology and homogeneous distribution in the centrifugal

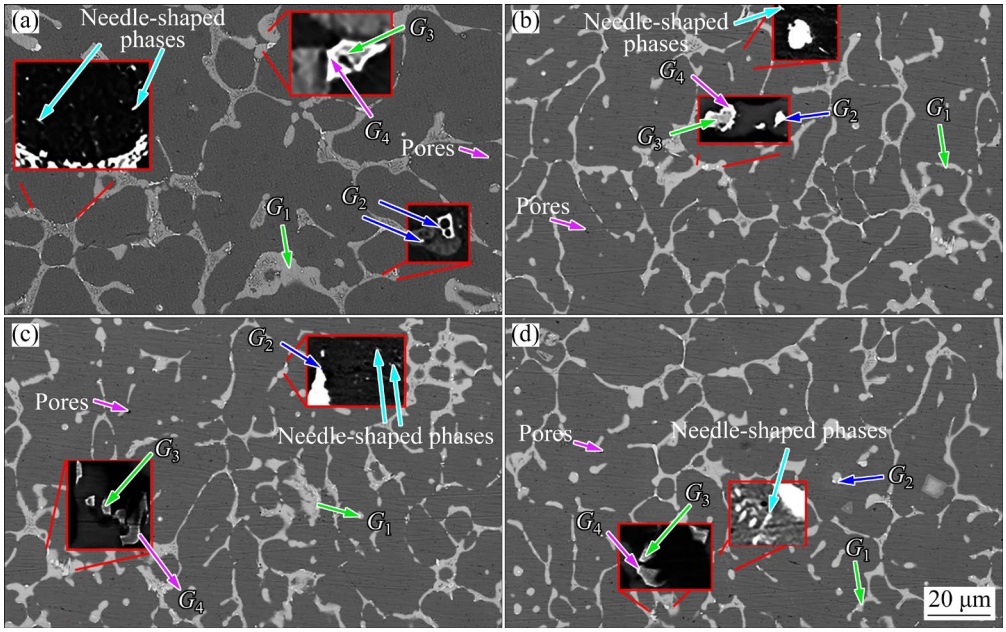

Fig. 7 SEM images of secondary phases on different sections of gravity-cast alloy: (a) 0 mm; (b) 4 mm-inner; (c) 8 mm; (d) 4 mm-outer

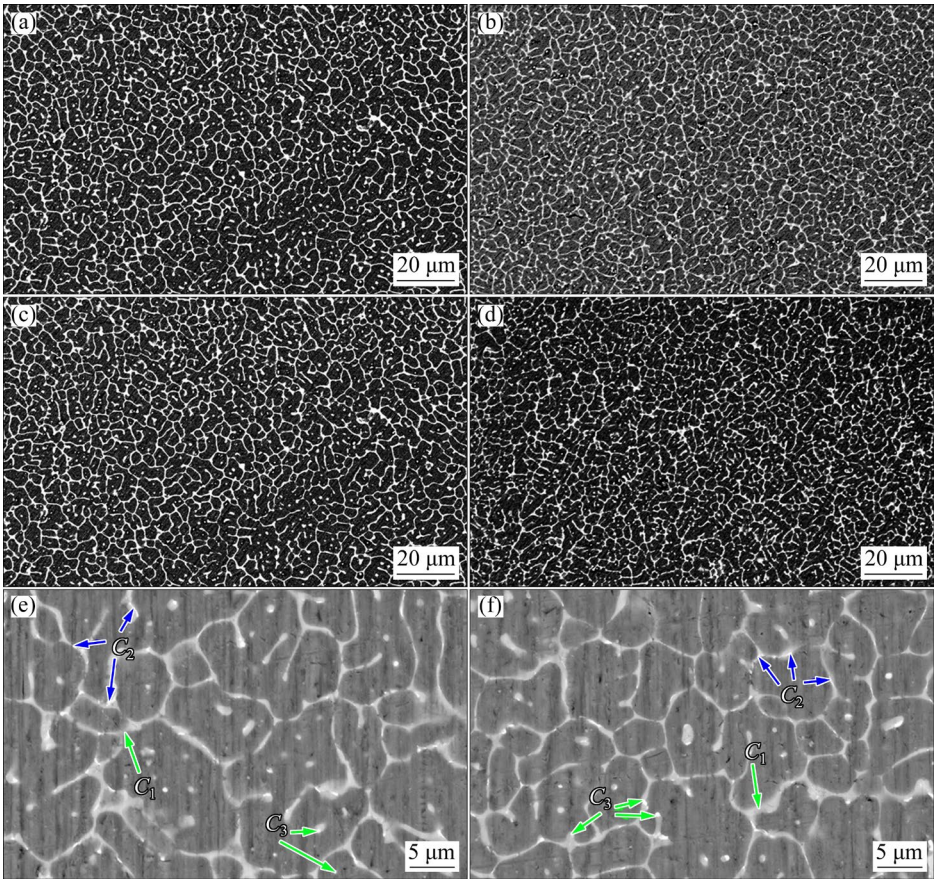

Fig. 8 SEM images of secondary phases on different sections of centrifugal-cast alloy: (a) 0 mm; (b, e) 4 mm-inner; (c) 8 mm; (d, f) 4 mm-outer

Table 2 Typical elemental compositions of secondary phases obtained by EDS or EPMA point analyses of different positions marked in Figs. 7 and 8

Specimen	Content/at.%					Secondary phase
	Al	Cu	Mg	Zn	Fe	
G_1	80.09	13.18	4.31	1.86	−	α(Al)+Al_6CuLi_3
G_2	65.79	32.08	0.98	1.12	−	Al_2Cu
G_3	73.98	3.88	0.11	0.16	21.82	$Al_{13}Fe_4$
G_4	69.35	19.32	0.21	0.35	9.91	Al_7Cu_2Fe
G-matrix	98.83	0.29	0.32	0.13	0.005	
C_1	80.98	13.54	4.13	1.42	−	α(Al)+Al_6CuLi_3
C_2	65.98	32.07	0.87	1.03	−	Al_2Cu
C_3	72.62	3.92	0.11	0.16	22.56	$Al_{13}Fe_4$
C-matrix	98.82	0.63	0.38	0.23	0.016	

casting point towards superior control the secondary phase characteristics compared to the gravity-cast alloy.

Figure 9 shows the volume fraction of secondary phases on different sections of both gravity and centrifugal castings. According to quantitative statistics, the volume fractions of Al_6CuLi_3, Al_2Cu and $Al_{13}Fe_4$/Al_7Cu_2Fe phases in the gravity casting progressively increase with decreasing height. However, the centrifugal casting exhibits a relatively

Table 3 Average diameter/thickness of secondary phases of gravity-cast and centrifugal-cast alloys

Phase	Diameter/thickness of gravity casting/μm	Diameter/thickness of centrifugal casting/μm
α(Al)+Al_6CuLi_3	4.38	0.68
Al_2Cu	2.77	0.41
$Al_{13}Fe_4$/Al_7Cu_2Fe	2.28	0.28

homogeneous distribution of secondary phases, including Al_6CuLi_3, Al_2Cu and $Al_{13}Fe_4$ phases, despite their higher volume fractions at the 4 mm-outer in comparison to the other sections. Moreover, compared with the gravity casting, the centrifugal casting exhibits an elevated volume fraction of the Al_6CuLi_3 phase, accompanied by a reduction in the volume fraction of Al_2Cu and $Al_{13}Fe_4$/Al_7Cu_2Fe phases.

Table 4 Quantitative proportions of secondary phases with different morphologies in gravity-cast and centrifugal-cast alloys

Phase	Quantitative proportion/%	
	Gravity casting	Centrifugal casting
Irregular Al_2Cu	61.80	11.90
Spherical Al_2Cu	38.20	88.10
Platelet-like $Al_{13}Fe_4$/Al_7Cu_2Fe	56.80	1.90
Spherical $Al_{13}Fe_4$/Al_7Cu_2Fe	43.20	98.10

Figure 10 presents TEM images including the bright field (BF) images and SAED patterns of intermetallic compounds in both gravity-cast and centrifugal-cast alloys. The intermetallic compounds in both alloys, characterized by five-fold symmetry patterns (Figs. 10(a) and (c)), are associated with the quasi-crystalline T_2 phase. This equilibrium T_2

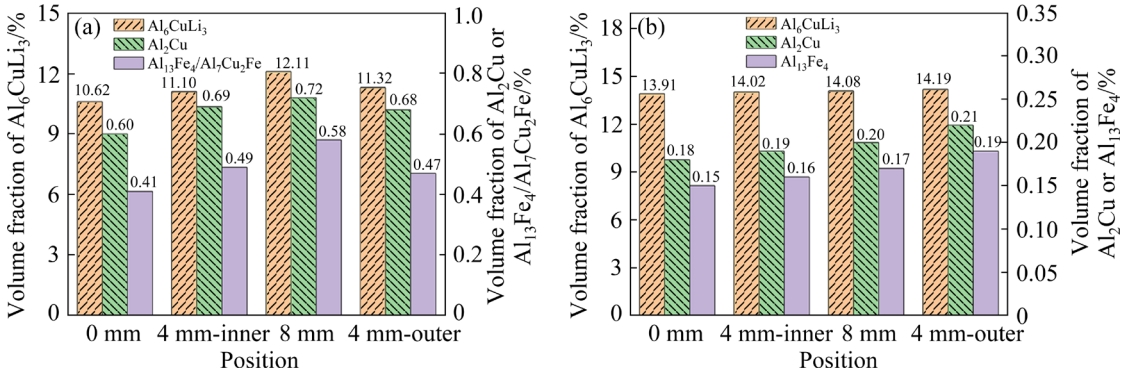

Fig. 9 Volume fraction of secondary phases on different sections of gravity (a) and centrifugal (b) castings

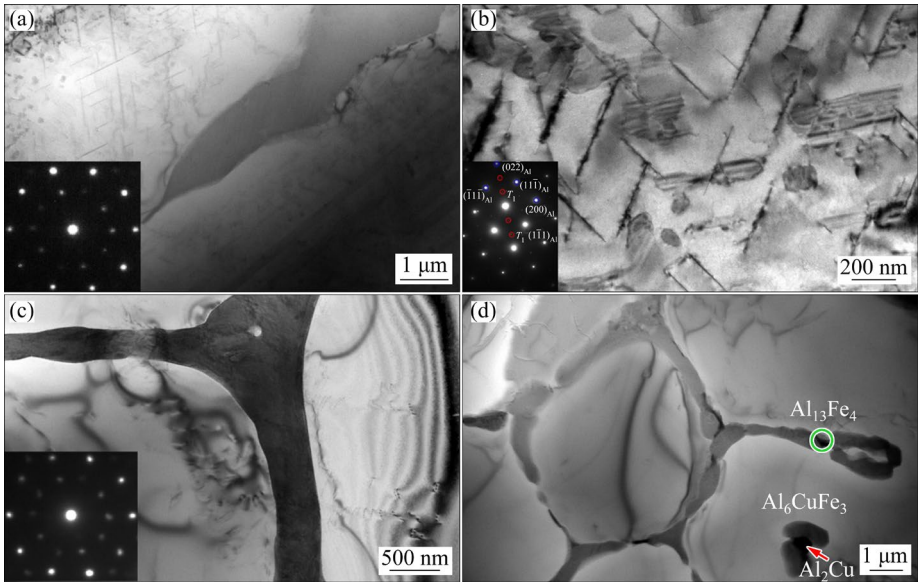

Fig. 10 TEM images of secondary phases in Al−Cu−Li−Mg−Zn alloys (SAED patterns of T_2 phase show typical five-fold symmetry in (a) and (c); SAED pattern in (b) is taken near $[011]_{Al}$ zone axis): (a, b) Gravity-cast alloy; (c, d) Centrifugal-cast alloy

phase is one of the most common secondary phases observed at grain boundaries in Al−Li−Cu-based alloy [13]. The plate-shaped phase (the needle-shaped phase in Fig. 7) with a length of 300−1100 nm is also observed within the α(Al) matrix in the gravity-cast alloy, as shown in Fig. 10(b). The spots at $1/3(02\bar{2})_{Al}$ and their equivalent positions in SAED pattern are straightforward to identify as T_1 (Al_2CuLi) phase. This T_1 phase is considered to be the most important strengthening phase in Al−Cu−Li alloys. However, no T_1 phase is observed in the centrifugal-cast alloy, as evident from Figs. 10(c) and (d). The centrifugal-cast alloys are mainly composed of Al_6CuLi_3, Al_2Cu and $Al_{13}Fe_4$ phases in the intercellular/dendritic regions (Fig. 10(d)), which are consistent with the experimental results of XRD patterns (Fig. 6) and SEM images (Fig. 8).

3.4 Mechanical properties

Figure 11(a) presents the engineering stress−strain curves of both gravity-cast and centrifugal-cast alloys and the corresponding mechanical properties are given in Table 5. The gravity-cast alloy fractures during the elastic deformation stage, demonstrating inferior tensile properties. However, the centrifugal-cast alloy shows a much better combination of tensile properties with an UTS of 342.4 MPa, a YS of 292.0 MPa, and an EL of 6.1%. Figure 11(b) and Table 5 offer a comparative analysis of tensile properties for the centrifugal-cast alloy in comparison to reported Al−Cu−Li alloys fabricated by different solidification or hot-extruded techniques [8,9,14−19]. Notably, the centrifugal-cast alloy exceeds the YS of previously reported alloys while still retaining a reasonable level of EL, thus exemplifying a noteworthy combination of high strength and moderate ductility. Importantly, the water-cooling centrifugal casting technique achieves these superior mechanical properties without requiring complicated heat treatment or deformation processing, offering significant cost reduction in the production of Al−Cu−Li alloys.

Table 5 Room-temperature tensile properties of gravity-cast and centrifugal-cast alloys

Method	UTS/MPa	YS/MPa	EL/%
Gravity casting	221.9	221.9	−
Centrifugal casting	342.4	292.0	6.1

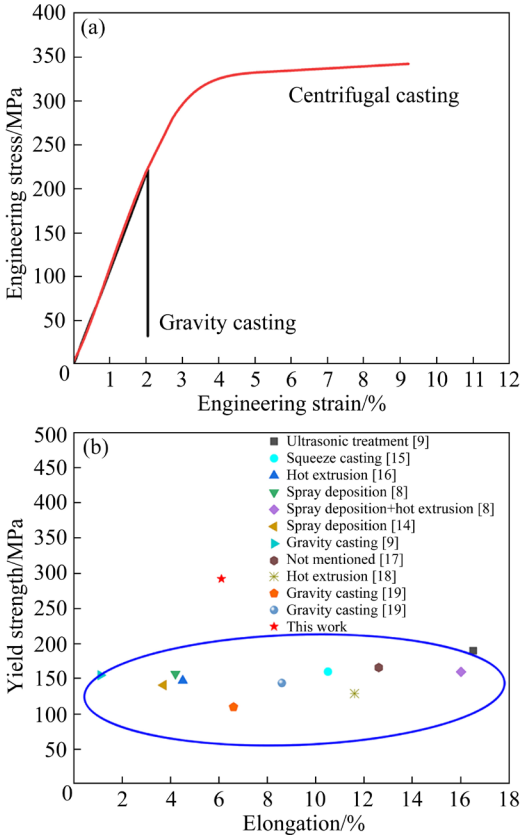

Fig. 11 Engineering stress−stain curves of gravity-cast and centrifugal-cast alloys at room temperature (a) and comparison between mechanical properties of investigated alloys and partially reported Al−Cu−Li alloys [8,9,14−19] (b)

3.5 Fractographs

The SEM fractographs and side views of both gravity-cast and centrifugal-cast samples after tensile tests are presented in Fig. 12. The failure surface of the gravity-cast alloy exhibits numerous micro-cracks, voids and fractured secondary phases, as depicted in Fig. 12(a). These characteristics are indicative of a brittle fracture mode, with no evident indications of ductile behavior. The presence of cleavage planes within secondary phases along the grain boundaries identifies them as brittle intermetallic compounds. As illustrated in Fig. 12(b), the Fe-bearing $Al_{13}Fe_4$/Al_7Cu_2Fe phase at grain boundaries contains large amounts of micro-cracks, acting as preferential sites for micro-crack nucleation. These micro-cracks then propagate along grain boundaries due to the brittle nature of the eutectic phase, which is the most energy-efficient path for the crack propagation. Moreover, voids within the matrix (Figs. 7 and 12(a)) promote transgranular fracture. The porosity and coarse

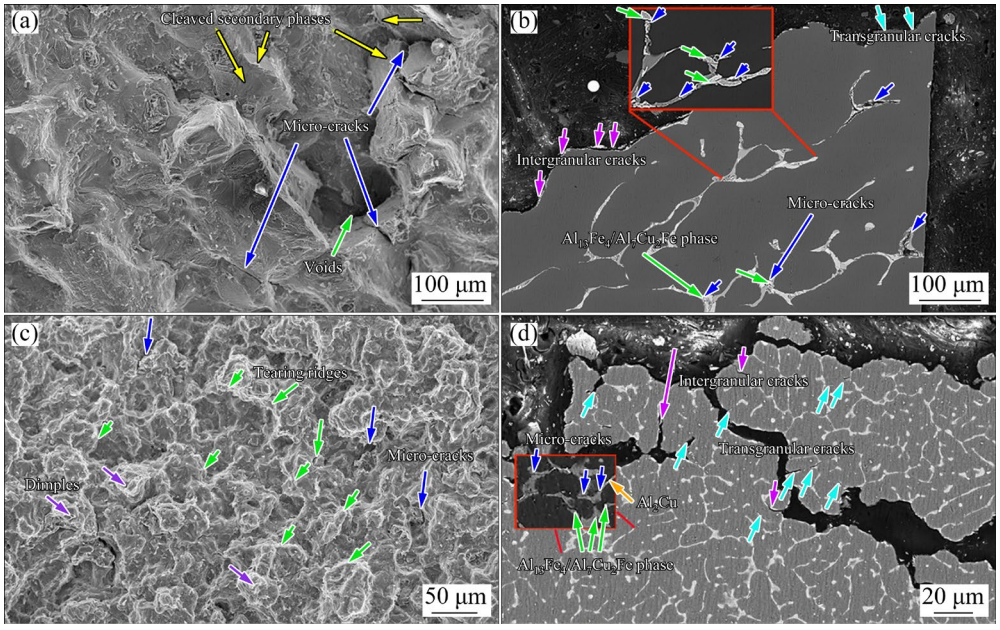

Fig. 12 SEM fractographs (a, c) and fracture profiles (b, d) of gravity-cast (a, b) and centrifugal-cast (c, d) alloys

$Al_{13}Fe_4$/Al_7Cu_2Fe phase lead to a mixed transgranular and intergranular fracture mode, as shown in Fig. 12(b). The fracture surfaces of the centrifugal-cast alloy exhibit a lot of tearing ridges, a few small dimples, and microcracks, indicative of a more ductile behavior compared to the gravity-cast alloy (Fig. 12(c)). Observing the side views of the fractured surface in Fig. 12(d) reveals that the fine dispersed Al_2Cu and $Al_{13}Fe_4$ phases within the centrifugal-cast alloy do not manifest microcracks. Instead, micro-cracks in the centrifugal-cast alloy predominantly originate within the eutectic phase. These micro-cracks extend not only along the eutectic phase at the grain boundary but also propagate into the grain interior facilitated by the presence of fine dendrites. This results in a mixed transgranular and intergranular fracture mode.

4 Discussion

4.1 Microstructure

4.1.1 Microstructure formation in gravity casting

The solidification process in the gravity-cast alloy is schematically illustrated in Fig. 13. Initially, at temperatures exceeding the liquidus temperature, the alloy remains in a liquid state, as shown in Fig. 13(a). As the temperature decreases, the α(Al) phase precipitates as the initial solid phase during solidification. Solute atoms are continuously rejected from the nucleated α(Al) at the solidifying interface (Fig. 13(b)) since the distribution coefficient (k) of Cu, Mg, Zn and Fe elements is 0.17, 0.31, 0.48 and 0.14 (k<1), respectively [20−23]. Inadequate diffusion of solute atoms in the molten liquid results in the accumulation of excessive solute atoms at the solid−liquid interface, causing severe micro-segregation (Fig. 5).

Further cooling leads to the generation of the $Al_{13}Fe_4$ phase through a eutectic reaction (L=α(Al)+$Al_{13}Fe_4$) (Fig. 13(c)), as reported in the 8090 Al−Li alloy [20]. Subsequently, the $Al_{13}Fe_4$ phase undergoes a peritectic transformation, resulting in the formation of the Al_7Cu_2Fe phase as reported in Ref. [12]. The presence of the Al_7Cu_2Fe phase hinders subsequent peritectic reactions, resulting in the emergence of a core−shell configuration, as illustrated in Figs. 7 and 13(d). Additionally, massive pile-ups of solute atoms like Cu, Mg, Zn and Fe at the solid−liquid interface cause constitutional undercooling, which promotes the appearance of coarse dendrites (Figs. 2(a−d)). With further temperature reduction, Cu concentration exceeds the critical value of eutectic composition, which leads to the generation of α(Al)+Al_2Cu andα(Al)+T_2 eutectics along the grain boundaries/dendritic regions, respectively (Fig. 13(e)). With the continued decrease in temperature, the liquid phase has completely transformed into the solid phase and then the solid-state phase transformation always takes place. The plate-shaped T_1 phase (Figs. 7 and 10(b)) precipitates within the grain interiors (Fig. 13(f)).

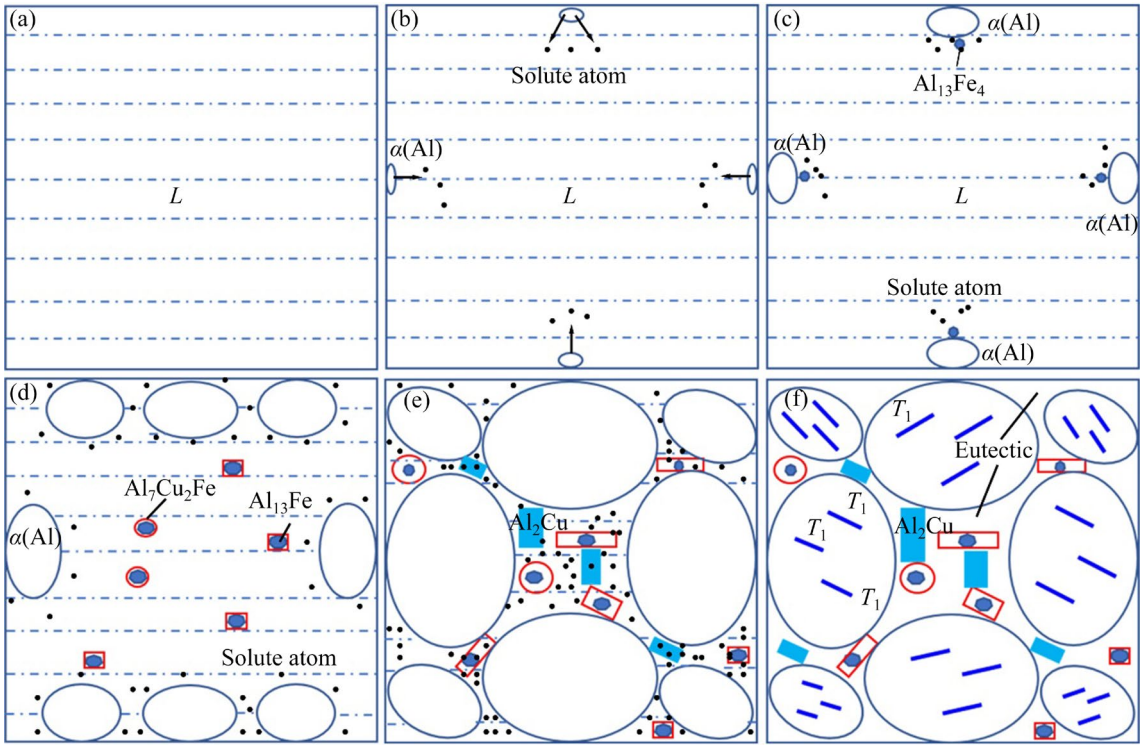

Fig. 13 Schematic illustration of solidification process of gravity-cast alloy

The gravity-induced segregation of Cu, Mg, Zn and Fe elements in the gravity-cast alloy (Figs. 4(a−d)) is influenced by the varying densities of these elements, and the relatively slow cooling rate. This gravitational segregation contributes to the formation of an inhomogeneous microstructure in the gravity-cast alloy. Primarily, the gravitational segregation leads to a gradual increase in the volume fraction of secondary phases as the height decreases (Fig. 9). Furthermore, the gravitational segregation results in a gradual increase in constitutional undercooling, leading to an increased number of dendrites with decreasing height (Figs. 2(a−c)).

4.1.2 Microstructure formation in centrifugal casting

The influencing factors of water-cooled centrifugal casting on microstructure can be classified into four distinct categories [7]: centrifugal force, fluid dynamics, vibration and rapid solidification. The centrifugal force generated by the rotating apparatus is 107−109 times greater than the natural gravity force. This strong centrifugal force exerts a significant impact on the liquid melt, which alleviates gravity segregation dramatically (Figs. 4 and 9) during the centrifugal casting process. Furthermore, the centrifugal force effectively removes rejected solute atoms from the solidification front, promoting a homogeneous dispersion of solute atoms throughout the melt. This process markedly reduces the solute concentration gradient and constitutional undercooling. The resulting small solute concentration gradient leads to a low CSR value of Cu, Mg, Zn and Fe elements (Fig. 5). Furthermore, the small constitutional undercooling hampers the development and expansion of dendritic structures (Figs. 2(e−h)) and secondary phases such as Al_2Cu and $Al_{13}Fe_4$ (Fig. 8) while favoring the formation of equiaxed grains (Figs. 2(e−h)).

The intense backflow phenomenon arises from the substantial collision between the molten metal and mold wall or solid−liquid interface (Figs. 14(a−e)). This vigorous backflow causes dendrites, columnar grains and secondary phases near the mold wall or solid−liquid interface to undergo mechanical fragmentation, dispersing them within the liquid metal (Figs. 14(c−e)). Upon contact with freshly hotter molten metal (Fig. 14(c)), these fragments can either melt again, disappear or collide, generating new smaller fragments. These newly formed fragments, uniformly transported into the bulk liquid, serve as nuclei for the generation of fine equiaxed grains or secondary phases, exhibiting a multiplication effect (Figs. 14(c−e)).

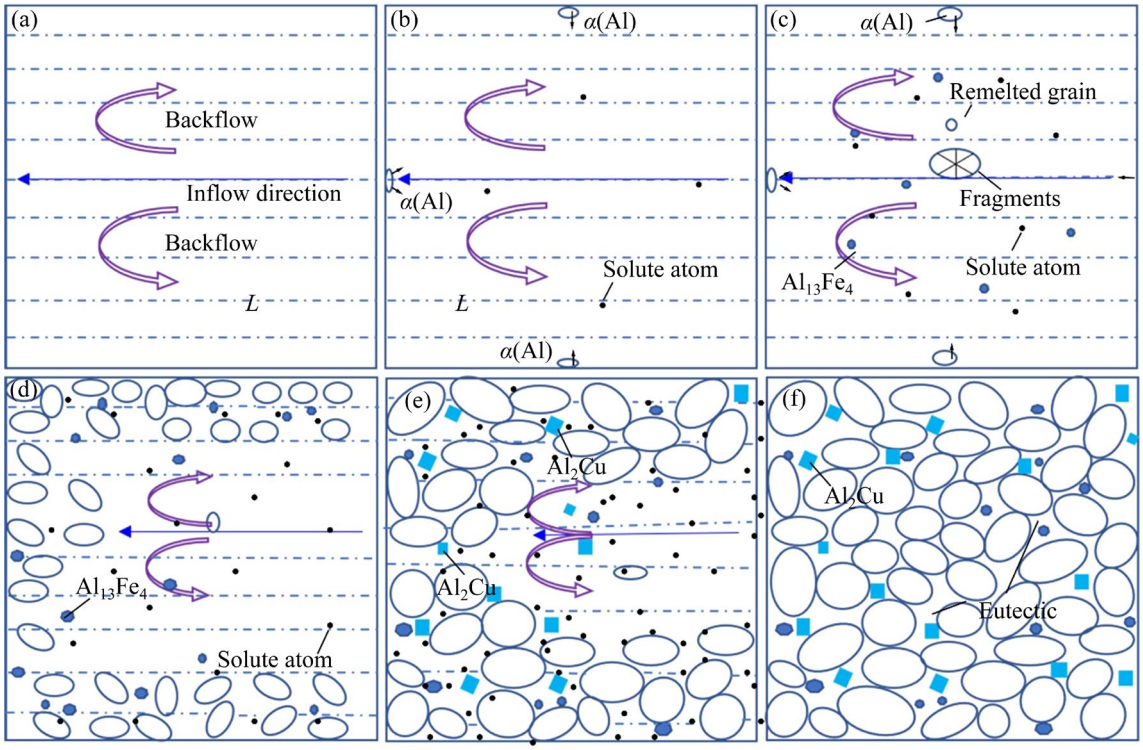

Fig. 14 Schematic illustration of solidification process of centrifugal-cast alloy

Compared to the backflow, the centrifugal field is relatively weak but exerts a continuous and prolonged influence on the microstructure. This field induces gradients in grain and particle size, and chemical compositions along the direction of the centrifugal force, driven by density discrepancies. The backflow, however, stems from an instantaneous substantial impact followed by gradual attenuation. The robust stirring action caused by this intense backflow significantly mitigates the macro-segregation of Cu, Mg, Zn and Fe elements induced by both the centrifugal and gravitational fields (Figs. 4(e−h)).

Strong vibration is also generated due to the inherent vibration effect of the centrifugal apparatus [24]. Furthermore, the water-cooled copper mold employed in the centrifugal casting technology facilitates efficient rapid solidification, resulting in a considerably high cooling rate (~3×10^2 K/s) compared to that of the gravity casting (~10^1 K/s). Vibration and rapid solidification are responsible for promoting nucleation and refining grains, contributing to the development of a more homogeneous microstructure (Fig. 14(f)). Therefore, the centrifugal-cast alloy also exhibits a fine and homogeneous microstructure such as grains (Fig. 2) and secondary phases such as Al_2Cu and $Al_{13}Fe_4$ phases (Fig. 7).

In general, the T_1 phase originates from solid-phase transformation during the latter stage of solidification in the Al−Cu−Li−Mg−Zn alloy. Furthermore, the development of the Al_7Cu_2Fe phase involves a peritectic reaction between the liquid and $Al_{13}Fe_4$ phases [12]. To generate the T_1 and Al_7Cu_2Fe phases, adequate diffusion time for Cu, Li and Fe elements is essential. In this study, the cooling rate of the gravity-cast alloy is notably lower compared to that of the centrifugal-cast alloy. Gravity casting, in contrast to centrifugal casting, offers more extensive diffusion time for Cu, Li and Fe elements. As a result, T_1 and Al_7Cu_2Fe phases are present in the gravity-cast alloy while absent in the centrifugal-cast alloy.

4.2 Mechanical properties

The presence of pores during the casting process is a common phenomenon in metallurgy, which significantly deteriorates the quality of the as-cast alloy. Addressing and minimizing casting porosity in Al−Li alloys constitute a current focal point of research [9]. The gravity-cast alloy is particularly susceptible to generating porosity during the casting process (Fig. 7). Porosity defects coupled with the presence of the coarse Fe-bearing

$Al_{13}Fe_4$/Al_7Cu_2Fe phase (Figs. 12(a) and (b)) can lead to localized stress concentration, making the gravity-cast alloy more susceptible to failure under tension (Fig. 11(a)). The centrifugal casting technology, however, is one of the most effective ways to avoid porosity in the Al−Li alloy (Fig. 8). Maintaining substantial centrifugal force is crucial for minimizing porosity defects in the as-cast Al−Li alloy during the filling process of liquid metal. Additionally, the vibration that acts on the melt enhances the metal feeding and thus reduces the porosity [24]. WEI et al [25] concluded that there are relatively large normal and shear stress concentrations around the pores, indicating that cracks prefer to appear in these regions. Consequently, the decrease in porosity defects in the centrifugal-cast alloy can significantly improve its comprehensive mechanical properties.

4.2.1 Enhancement of YS

The centrifugal-cast alloy exhibits notably higher YS compared with the gravity-cast alloy (Fig. 11 and Table 5), which may be attributed to two aspects: grain boundary strengthening (GBS) and solid solution strengthening (SSS). Based on polycrystalline materials with different grain orientations and deformation complexities, the YS related to the critical resolved shear stress (CRSS) can be described as the following expression [26]:

$$\sigma_{0.2}=\sigma_{GBS}+M(\tau_m+\tau_{ss}) \quad (2)$$

where $\sigma_{0.2}$ is the YS of the centrifugal-cast alloy. σ_{GBS} is the grain boundary strengthening effect. The Taylor factor M is about 3.1 for materials exhibiting a relatively weak texture. τ_m is the intrinsic CRSS of the Al matrix, which is about 10 MPa for materials without deformation [27]. τ_{ss} is the solid solution strengthening effect.

Based on the Hall−Petch relationship, the strengthening contribution arising from GBS can be expressed as follows:

$$\sigma_{GBS}=\sigma_0^{Al}+Kd_G^{-0.5} \quad (3)$$

where σ_0^{Al} is the friction stress of pure Al and its value is 10 MPa [28], and K is a constant dependent on the contribution of grain boundaries to the relative strength of materials. The value of K is 0.08 MPa·$m^{0.5}$ for the Al alloy [29]. d_G is the average grain size. The YS contribution arising from GBS is estimated to be 35.7 MPa for the Al−Cu−Li−Mg−Zn alloy.

SSS involves the hindering effect of dislocation movement mainly caused by the lattice distortion of solute atoms such as Cu, Mg, Zn and Li within the matrix in the Al−Cu−Li−Mg−Zn alloy. The value of τ_{ss} is 72.7 MPa based on Table 5 and Eq. (4). The strengthening contributions can thus be shown in Fig. 15. The strength values for GBS and SSS are 35.7 and 225.3 MPa, respectively.

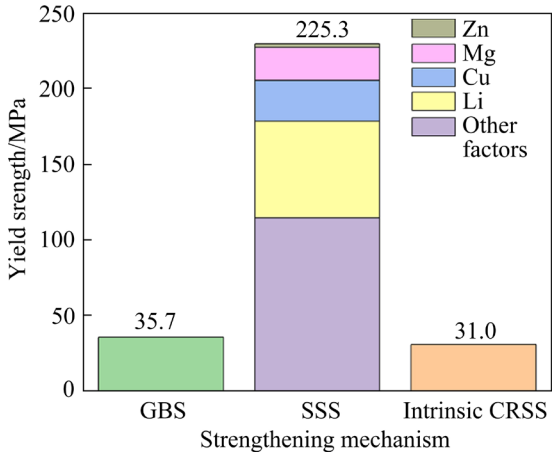

Fig. 15 Main strengthening contributions to YS of centrifugal-cast alloy

The YS involved in SSS is measured by [30]

$$\tau_{ss}=\tau_{trace}+\sum_i(k_i\cdot c_{ss,i}^m) \quad (4)$$

where τ_{trace} is the strengthening effect caused by other elements such as Zr and Fe, dendrites and Al_3Zr particles, and its value is 37 MPa [31]. $c_{ss,i}^m$ is the solute concentration of element i in the matrix. k_i is the scaling factor of element i that describes the solute−dislocation interaction. m is a constant whose value can be 2/3 or 1 [30]. In this study, the value of m is 1.

Cu, Mg and Zn contents in the α(Al) matrix of the centrifugal-cast alloy are 0.63%, 0.38% and 0.23%, respectively (Table 2). According to the previous work, the scaling factors of Cu, Mg and Zn elements were determined: k_{Cu}=13.8 MPa·wt.%$^{-1}$, k_{Mg}=18.6 MPa·wt.%$^{-1}$ and k_{Zn}=2.9 MPa·wt.%$^{-1}$ [28]. The strengthening contribution from Cu, Mg and Zn elements to the solid solution effect (τ_{ss}) is 8.7, 7.1 and 0.7 MPa, respectively. Based on Table 5 and Eqs. (2)−(4), the τ_{ss} of Li atoms is about 20.6 MPa. Li element has a larger contribution to the SSS than other elements such as Cu, Mg and Zn. This is primarily attributed to the comparatively high solid solubility of Li in the Al matrix, retaining a content of 4−5 at.% even after prolonging aging treatment [32]. Furthermore, Li atoms in the Al

matrix induce substantial lattice strain due to the significant radius disparity between Li and Al atoms.

In the centrifugal-cast alloy, the volume fraction of the Al_6CuLi_3 phase (13.91%−14.19%) considerably surpasses that of other secondary phases including Al_2Cu and $Al_{13}Fe_4$ phases (0.33%−0.40%), as shown in Fig. 9. It is reasonably speculated that the Al matrix and Al_6CuLi_3 phase contain the majority of Cu and Li atoms. Based on the total Li contents in Table 1 and the Li contents within the Al_6CuLi_3 phase, the Li content in the matrix can be estimated to be 2.62 wt.%. Consequently, the value of k_{Li} based on the calculations in this study is 7.9 MPa·wt.%$^{-1}$.

4.2.2 Enhancement of EL

Compared with the gravity-cast alloy, the enhancement of EL in the centrifugal-cast alloy is attributed primarily to the following factors. The first factor is the refinement, morphological transformation and homogeneous distribution of secondary phases. Griffith fracture criteria are employed to describe the rapid extension of a crack in a homogeneous elastic body such as the Al alloy. The equation between the critical stress of crack propagation (σ_c) and the length of the initial crack (C) can be described as $\sigma_c=(2E\gamma/\pi C)^{0.5}$, where E denotes Young's modulus of secondary phases, and γ denotes fracture surface energy that is a measure of resistance to the initiation of crack propagation. Based on Griffith fracture criteria, the coarse secondary phases in the gravity-cast alloy are more prone to generating internal defects compared to the nano-scale secondary phases such as Al_6CuLi_3, Al_2Cu and $Al_{13}Fe_4$ phases in the centrifugal-cast alloy. Moreover, the gravity-cast alloy's coarse plate-like $Al_{13}Fe_4$/Al_7Cu_2Fe phase is inclined to generate stress concentration and has a limited capacity to absorb energy during the plastic deformation [33], making it susceptible to serving as the site of crack initiation. However, the fine, spherical and homogeneously distributed Al_2Cu and $Al_{13}Fe_4$ phases of the centrifugal-cast alloy do not exhibit microcracks (Fig. 12). Thus, the refinement, spheroidization and homogeneous distribution of Al_2Cu and $Al_{13}Fe_4$ phases are beneficial to the improvement of the EL of the centrifugal-cast alloy. The second factor is the fine equiaxed grains due to the centrifugal casting technique combined with rapid solidification. Fine grains exhibit homogeneous slip behavior under plastic deformation, resulting in a delayed fracture in the specimen [34]. Furthermore, the centrifugal-cast alloy also exhibits a relatively narrow grain size distribution (Fig. 3) and minimal macro-segregation and micro-segregation of Cu, Mg, Zn and Fe elements (Figs. 4 and 5). These characteristics impede detrimental strain localization while promoting coordinated deformation across the grains.

5 Conclusions

(1) The gravity-cast alloy exhibits an inhomogeneous microstructure characterized by large equiaxed α(Al) grains (131.6 μm) and coarse secondary phases. In contrast, the centrifugal-cast alloy displays a homogeneous and compact microstructure featuring fine equiaxed grains (9.7 μm) and secondary phases.

(2) The centrifugal-cast alloy exhibits a significant reduction in porosity, and macro- and micro-segregation of Cu, Mg, Zn and Fe elements compared with the gravity-cast alloy.

(3) In the gravity-cast alloy, coarse secondary phases are distributed unevenly within the sample, consisting of semi-continuous α(Al)+Al_6CuLi_3 phase, irregular Al_2Cu phase, platelet-like core−shell structure ($Al_{13}Fe_4$/Al_7Cu_2Fe) in intercellular/dendritic regions, and T_1 phase within grain interiors. However, the centrifugal-cast alloy exhibits fine and homogeneously dispersed secondary phases, including continuous α(Al)+Al_6CuLi_3, spherical Al_2Cu and $Al_{13}Fe_4$ phases.

(4) The gravity-cast alloy's poor mechanical properties were attributed to porosity defects and the presence of coarse plate-like $Al_{13}Fe_4$/Al_7Cu_2Fe phases. However, the centrifugal-cast alloy demonstrates impressive mechanical properties with an UTS of 342.4 MPa, an YS of 292.0 MPa and an EL of 6.1%. YS contributions of 35.7 MPa from GBS and 225.3 MPa from SSS are noted, with Li making the most significant contribution to SSS (scaling factor: 7.9 MPa·wt.%$^{-1}$).

(5) The centrifugal-cast alloy's EL is notably improved through a reduction in casting porosity and segregation, refinement and morphological transformation of secondary phases as well as the presence of fine equiaxed grains within a narrow size distribution.

CRediT authorship contribution statement

Qing-bo YANG: Conceptualization, Investigation, Formal analysis, Methodology, Writing − Original draft; **Wen-jing SHI:** Formal analysis, Validation; **Wen LIU:** Formal analysis; **Miao WANG:** Methodology; **Wen-bo WANG:** Data curation; **Li-na JIA** and **Hu ZHANG:** Supervision, Funding acquisition.

Declaration of competing interest

The authors declare that they have no known competing financial interests or personal relationships that could have appeared to influence the work reported in this paper.

Acknowledgments

This research was financially supported by the Natural Science Foundation of Ningbo, China (No. 2023J053). We express gratitude to Chu-nan LI from the Norwegian University of Science and Technology and Wei WEI from Ningbo MaterChem Technology Co., Ltd., as well as our fellow researchers at the Research Center for Lightweight Materials, Ningbo Institute of Technology, Beihang University, China.

References

[1] ZHANG Jin-shuo, ZHONG Xiao-xiang, ZHANG Ling, WU Guo-hua, LIU Wen-cai. Effect of heat treatments on microstructure and mechanical properties of sand cast Al−2Li−2Cu−0.5Mg−0.2Sc−0.2Zr alloy [J]. Transactions of Nonferrous Metals Society of China, 2022, 32(2): 411−423.

[2] WEN Feng, CHEN Ji-qiang, HAN Shuang, ZHOU Zi-xiang, ZHONG Shi-biao, ZHANG Ying-hui, LI Wei-rong, GUAN Ren-guo. Effect of crystal orientations and precipitates on corrosion behavior of Al−Cu−Li single crystals [J]. Transactions of Nonferrous Metals Society of China, 2022, 32(12): 3887−3900.

[3] YANG Qing-bo, DENG Yan-jun, YANG Mou, ZHANG Zhi-qing, LI Wei-guo, LIU Qing. Effect of Al_3Zr particles on hot compression behavior and processing map for Al−Cu−Li based alloys at elevated temperatures [J]. Transactions of Nonferrous Metals Society of China, 2020, 30(4): 872−882.

[4] SUN Jiang-wei, WU Guo-hua, ZHANG Liang, ZHANG Xiao-long, LIU Long-ling, ZHANG Jin-shuo. Microstructure characteristics of an ultra-high strength extruded Al−4.7Cu−1Li−0.5Mg−0.1Zr−1Zn alloy during heat treatment [J]. Journal of Alloys and Compounds, 2020, 813: 152216−152228.

[5] YANG Qing-bo, SHI Wen-jing, WANG Miao, JIA Li-na, WANG Wen-bo, ZHANG Hu. Influence of cooling rate on the microstructure and mechanical properties of Al−Cu−Li−Mg−Zn alloy [J]. Journal of Materials Research and Technology, 2023, 25: 3151−3166.

[6] LI Shi-ju, JIANG Tao, WANG Jin-yuan, CHEN Li-zheng, WEI Bo-wen, LI Yang, XU Guang-ming, WANG Zhao-dong. Effects of different external fields on the microstructure and mechanical properties of novel Al−Cu−Li alloy during twin-roll casting [J]. Materials Science and Engineering A, 2019, 757: 14−22.

[7] YEH J W, JONG S H. The cast structure of a 7075 alloy produced by a water-cooling centrifugal casting method [J]. Metallurgical and Materials Transactions A, 1994, 25(3): 643−650.

[8] WANG Yong-xiao, ZHAO Guo-qun, XU Xiao, CHEN Xiao-xue, ZHANG Wen-dong. Microstructures and mechanical properties of spray deposited 2195 Al−Cu−Li alloy through thermo-mechanical processing [J]. Materials Science and Engineering A, 2018, 727: 78−89.

[9] LI Jian-yu, PAN Yu, ZHAO Di-jia, LÜ Shu-lin, WU Shu-sen, GUO Wei. Development of a novel high strength and toughness Al−Cu−Li alloy casting billet with a new process [J]. Materials Science and Engineering A, 2022, 854: 143827−143834.

[10] TIAN Qing-le, DENG Kai, XU Zhi-shuai, HAN Ke, ZHENG Hong-xing. Microstructural characterization and mechanical property of Al−Li plate produced by centrifugal casting method [J]. Metals, 2021, 11(6): 966−975.

[11] MONDAL C, MUKHOPADHYAY A K. On the nature of $T(Al_2Mg_3Zn_3)$ and $S(Al_2CuMg)$ phases present in as-cast and annealed 7055 aluminum alloy [J]. Materials Science and Engineering A, 2005, 391(1/2): 367−376.

[12] PHRAGMEN G. On the phases occurring in alloys of Al with Cu, Mg, Mn, Fe and Si [J]. The Journal of the Institute of Metals, 1950, 77: 489−552.

[13] MUKHOPADHYAY A K, ZHOU D S, YANG Q B. Effect of variation in the Cu:Mg ratios on the formation of T_2 and C phases in AA 8090 alloys [J]. Scripta Metallurgica et Materialia, 1992, 26(2): 237−242.

[14] PU Qing-qing, JIA Zhi-hong, KONG Ya-ping, YANG Qing-bo, ZHANG Zhi-qing, FAN Xi, ZHANG Hao, LIN Lin, LIU Qing. Microstructure and mechanical properties of 2195 alloys prepared by traditional casting and spray forming [J]. Materials Science and Engineering A, 2020, 784: 139337−139347.

[15] LI Jian-yu, LÜ Shu-lin, WU Shu-sen, ZHAO Di-jia, GUO Wei. Micro-mechanism of simultaneous improvement of strength and ductility of squeeze-cast Al−Cu alloy [J]. Materials Science and Engineering A, 2022, 833: 142538−142546.

[16] LIN Yi, ZHENG Zi-qiao, LI Shi-chen, KONG Xxiang, HAN Ye. Microstructures and properties of 2099 Al−Li alloy [J]. Materials Characterization, 2013, 84: 88−99.

[17] KIM J H, JEUN J H, CHUN H J, LEE Y R, YOO J T, YOON J H, LEE H S. Effect of precipitates on mechanical properties of AA2195 [J]. Journal of Alloys and Compounds, 2016, 669: 187−198.

[18] CHEN Xiao-xue, ZHAO Guo-qun, LIU Guo-liang, SUN Lu, CHEN Liang, ZHANG Cun-sheng. Microstructure evolution and mechanical properties of 2196 Al−Li alloy in hot extrusion process [J]. Journal of Materials Processing Technology, 2020, 275: 116348−116361.

[19] WANG Yang, LI Zheng, YU Tian-fu, MEDJAHED A, WU Rui-zhi, HOU Le-gan, ZHANG Jing-huai, LI Xin-xin, ZHANG Mi-lin. Effect of Sc and Zr on microstructure and mechanical properties of as-cast Al−Li−Cu alloys [J]. Advanced Engineering Materials, 2018, 20(4): 1700898−17008105.

[20] LIU Y L, HU Z Q, ZHANG Y, SHI C X. The solidification behavior of 8090 Al−Li alloy [J]. Metallurgical Transactions B, 1993, 24(5): 857−865.

[21] HOU K H, BAESLACK W A. Effect of solute segregation

on the weld fusion zone microstructure in CO_2 laser beam and gas tungsten arc welds in Al−Li−Cu alloy 2195 [J]. Journal of Materials Science Letters, 1996, 15(3): 208−213.
[22] ZHANG Xin-xin, LIU Bing, ZHOU Xiao-rong, WANG Jun-jie, HASHIMOTO T, LUO Chen, SUN Zhi-hua, TANG Zhi-hui, LU Feng. Laser welding introduced segregation and its influence on the corrosion behaviour of Al−Cu−Li alloy [J]. Corrosion Science, 2018, 135: 177−191.
[23] LEI Xiao-wei, NUAM V L, BAI Yang, DANG Ren-ze, LI Wen-zhe, YAO Wen-jing, WANG Nan. Investigation on laser beam remelted Al−Cu−Li alloy. Part I: Segregation and aging behavior at grain and dendrite boundaries [J]. Journal of Alloys and Compounds, 2021, 855: 157519−157531.
[24] ABU-DHEIR N, KHRAISHEH M, SAITO K, MALE A. Silicon morphology modification in the eutectic Al−Si alloy using mechanical mold vibration [J]. Materials Science and Engineering A, 2005, 393(1/2): 109−117.
[25] WEI Zhi-yuan, DONG Xiao-xue, CAI Hong-neng, ZHAO Sheng-dun. Influences of the near-spherical 3D pore on failure mechanism of atmospheric plasma spraying TBCs using a macro-micro integrated model [J]. Surface and Coatings Technology, 2022, 437: 128375−128386.
[26] STARINK M J, WANG S C. A model for the yield strength of overaged Al−Zn−Mg−Cu alloys [J]. Acta Materialia, 2003, 51(17): 5131−5150.
[27] BARDEL D, PEREZ M, NELIAS D, DESCHAMPS A, HUTCHINSON C R, MAISONNETTE D, CHAISE T, GARNIER J, BOURLIER F. Coupled precipitation and yield strength modelling for non-isothermal treatments of a 6061 aluminium alloy [J]. Acta Materialia, 2014, 62: 129−140.
[28] MA K K, WEN H M, HU T, TOPPING T D, ISHEIM D, SEIDMAN D N, LAVERNIA E J, SCHOENUNG J M. Mechanical behavior and strengthening mechanisms in ultrafine grain precipitation-strengthened aluminum alloy [J]. Acta Materialia, 2014, 62: 141−155.
[29] MASUDA T, SAUVAGE X, HIROSAWA S, HORITA Z. Achieving highly strengthened Al−Cu−Mg alloy by grain refinement and grain boundary segregation [J]. Materials Science and Engineering A, 2020, 793: 139668−139679.
[30] GAZIZOV M, KAIBYSHEV R. Precipitation structure and strengthening mechanisms in an Al−Cu−Mg−Ag alloy [J]. Materials Science and Engineering A, 2017, 702: 29−40.
[31] RYEN Ø, HOLMEDAL B, NIJS O, NES E, SJÖLANDER E, EKSTRÖM H E. Strengthening mechanisms in solid solution aluminum alloys [J]. Metallurgical and Materials Transactions A, 2006, 37(6): 1999−2006.
[32] ARAULLO-PETERS V, GAULT B, GEUSER F D, DESCHAMPS A, CAIRNEY J M. Microstructural evolution during ageing of Al−Cu−Li−x alloys [J]. Acta Materialia, 2014, 66: 199−208.
[33] FANG X, SHAO G, LIU Y Q, FAN Z. Effects of intensive forced melt convection on the mechanical properties of Fe containing Al−Si based alloys [J]. Materials Science and Engineering A, 2007, 445-446: 65−72.
[34] TERLINDE G, LUETJERING G. Influence of grain size and age-hardening on dislocation pile-ups and tensile fracture for a Ti−Al alloy [J]. Metallurgical Transactions A, 1982, 13(7): 1283−1292.

水冷离心铸造技术改善 Al−Cu−Li−Mg−Zn 合金的显微组织与力学性能

杨庆波[1,2,3]，石文静[1]，刘 稳[2]，王 苗[2]，王文博[2]，贾丽娜[1,2]，张 虎[1,2]

1. 北京航空航天大学 材料科学与工程学院，北京 100191；
2. 北京航空航天大学 宁波创新研究院 轻质材料研究中心，宁波 315100；
3. 苏州实验室，苏州 215123

摘 要：研究传统重力铸造和和离心铸造结合快速凝固制备的铸态 Al−Cu−Li−Mg−Zn 合金的显微组织和力学性能。实验结果表明，与重力铸造相比，水冷离心铸造技术由于剧烈返流、离心力场、振动和快速凝固能显著降低孔隙率，细化 α(Al)晶粒和第二相，改变第二相的形貌并降低宏观和微观偏析程度。孔隙率和粗大的板状 $Al_{13}Fe_4$/Al_7Cu_2Fe 相导致重力铸造合金在达到屈服点之前断裂。然而，离心铸造合金具有超高屈服强度(292.0 MPa)和中等伸长率(6.1%)。这种超高的屈服强度归因于固溶强化(SSS)和晶界强化(GBS)的共同作用，其中，SSS 的贡献为 225.3 MPa，GBS 的贡献为 35.7 MPa。比例因子为 7.9 MPa·wt.%$^{-1}$ 的 Li 对 SSS 的贡献最大。通过降低孔隙率和偏析行为、细化显微组织以及改变第二相的形貌，可以有效提高离心铸造合金的伸长率。

关键词：Al−Cu−Li−Mg−Zn 合金；水冷离心铸造；显微组织；力学性能；偏析行为

(Edited by Wei-ping CHEN)